Journal of Power Sources 245 (2014) 830–835

Contents lists available at SciVerse ScienceDirect

Journal of Power Sources

journal homepage: www.elsevier.com/locate/jpowsour

Structure and properties of Li-ion conducting polymer gel electrolytes based on ionic liquids of the pyrrolidinium cation and the bis(trifluoromethanesulfonyl)imide anion

Jagath Pitawala [a], Maria Assunta Navarra [b], Bruno Scrosati [b], Per Jacobsson [a], Aleksandar Matic [a,*]

[a] Department of Applied Physics, Chalmers University of Technology, SE-41296 Göteborg, Sweden
[b] University of Rome La Sapienza, P.le Aldo Moro 5, 00185 Rome, Italy

HIGHLIGHTS

- The physical properties of the ionic liquid are influenced by the membrane confinement.
- Li-ion coordination, anion conformation, and T_g, change in the membrane.
- The crystallinity and crystal form are influenced by the membrane configuration.

ARTICLE INFO

Article history:
Received 28 April 2013
Received in revised form
19 June 2013
Accepted 8 July 2013
Available online 17 July 2013

Keywords:
Ionic liquids
PVdF-HFP gel polymer electrolytes
Ionic conductivity
Glass transition

ABSTRACT

We have investigated the structure and physical properties of Li-ion conducting polymer gel electrolytes functionalized with ionic liquid/lithium salt mixtures. The membranes are based on poly(vinylidene fluoride-co-hexafluoropropylene) copolymer, PVdF-HFP, and two ionic liquids: pyrrolidinium cations, N-butyl-N-methylpyrrolidinium (PyR_{14}^{+}), N-butyl-N-ethylpyrrolidinium (PyR_{24}^{+}), and bis(trifluoromethanesulfonyl) imide anion (TFSI). The ionic liquids where doped with 0.2 mol kg^{-1} LiTFSI. The resulting membranes are freestanding, flexible, and nonvolatile. The structure of the polymer and the interactions between the polymer and the ionic liquid electrolyte have been studied using Raman spectroscopy. The ionic conductivity of the membranes has been studied using dielectric spectroscopy whereas the thermal properties were investigated using differential scanning calorimetry (DSC).

These results show that there is a weak, but noticeable, influence on the physical properties of the ionic liquid by the confinement in the membrane. We observe a change in the Li-ion coordination, conformation of the anion, the fragility and a slight increase of the glass transition temperatures for IL/LiTFSI mixtures in the membranes compared to the neat mixtures. The effect can be related to the confinement of the liquid in the membrane and/or to interactions with the PVdF-HFP polymer matrix where the crystallinity is decreased compared to the starting polymer powder.

1. Introduction

Gel polymer electrolytes (GPEs) are potential candidates to be used as electrolyte membranes in high energy density rechargeable lithium batteries, fuel cells, solar cells, and electrochromic windows [1–8]. GPEs can be formed using many different polymer systems [1,2,4]. Among the different systems, poly(vinylidene fluoride-co-hexafluoropropylene) copolymer (PVdF-HFP) based membranes have received considerable attention since they can trap large amounts of a liquid electrolyte while retaining dimensional stability, flexibility, and transparency [1,2]. The large fraction of the liquid phase ensures a high ionic conductivity since the ion conduction takes place in the liquid phase in the GPEs. In addition, PVdF-HFP based membranes are thermally and chemically stable [2,3].

PVdF-HFP based GPEs was first proposed as lithium ion conducting electrolytes by Bellcore [9] and has since then been extensively used in lithium batteries [1]. Typically PVdF-HFP based GPEs are formed with conventional liquid electrolytes based on

* Corresponding author. Tel.: +46 31 7723352; fax: +46 31 772 2090.
E-mail address: matic@chalmers.se (A. Matic).

0378-7753/$ – see front matter © 2013 Elsevier B.V. All rights reserved.
http://dx.doi.org/10.1016/j.jpowsour.2013.07.045

lithium salt-doped organic solvents such as ethylene carbonate, propylene carbonate, dimethylcarbonate, or diethylcarbonate [1–4,9]. However, there are several problems associated with the conventional liquid electrolytes, such as flammability and volatility that limits the safety and reliability of the battery [2,10].

A promising recent approach to overcome these problems has been the replacement of the traditional electrolytes in the GPE membranes with electrolytes based on ionic liquids (ILs), which are nonvolatile, nonflammable, and can be designed to have large electrochemical windows [10–16]. Previous studies have mainly focused on the performance of the ionic liquid based GPEs in batteries and characterization of the transport properties. By selecting a suitable ionic liquid the cell performance with IL/GPE membranes can be improved in terms of capacity and cyclability [14,16]. For instance GPEs based on PVdF-HFP and pyrrolidinium and piperidinium bis(trifluoromethanesulfonyl)imide based ionic liquids have been investigated with respect to transport properties, electrochemical and thermal stability [11–13,16]. The results show an improvement of the ionic conductivity and a stabilization of the interface with the lithium electrodes with addition of a small amount of organic solvents such as ethylene, propylene, and dimethyl carbonates into the PVdF-HFP/IL/Li-salt GPEs. In addition, Ferrari et al. have characterized and discussed filler effects (different types of silica) on the ionic conductivity and the electrochemical properties in a GPE based on 30 wt% PVdF-HFP + 70 wt % (LiTFSI/PYRA$_{1201}$TFSI), where PYRA$_{1201}$ is N-ethyl(methylether)-N-methylpyrrolidinium [15]. However, there are so far no results reported on influence of the IL/Li-salt electrolyte on the polymer structure and the influence of the membrane on the microscopic state of the ionic liquid electrolyte.

In this work, we investigate the structure, properties and interactions in PVdF-HFP based GPEs incorporating IL/LiTFSI solutions based on pyrrolidinium cations, N-butyl-N-methylpyrrolidinium bis(trifluoromethanesulfonyl)imide (PyR$_{14}$TFSI) and N-butyl-N-ethylpyrrolidinium bis(trifluoromethanesulfonyl)imide (PyR$_{24}$TFSI), see Fig. 1, doped with 0.2 mol kg^{-1} LiTFSI. The membranes, prepared by solution casting, are characterized with respect to transport properties and thermal properties, polymer structure and ionic liquid membrane interactions. The aim of the study is to correlate the behavior of the macroscopic properties, such as conductivity and glass transition temperature, to the microscopic structure and interactions of the membrane and the ionic liquid electrolyte.

2. Experimental

2.1. Materials and sample preparation

The PyR$_{14}$TFSI ionic liquid (purity > 99%) and LiTFSI salt (purity 99.95%) were purchased from Solvionic and 3 M, respectively, and used as received. The PyR$_{24}$TFSI ionic liquid was synthesized following the procedure described in detail in reference 17. The IL/LiTFSI mixtures were prepared (in an argon dry box) by mixing 0.2 mol kg^{-1} of LiTFSI in the neat ionic liquids under magnetic stirring at 60 °C until homogenous solutions were obtained.

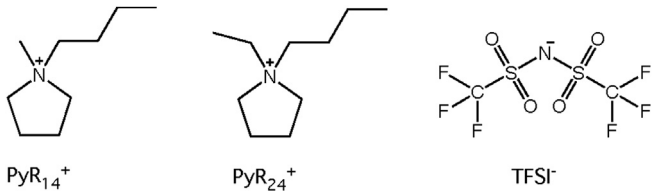

Fig. 1. Structure of the cations and the anion of the ionic liquids used in the GPE membranes.

The GPE membranes were prepared according to a solution casting procedure reported in Refs. [13,16]. First, PVdF-HFP (Kynar Flex 2801) was dissolved in acetonitrile. Thereafter, IL/LiTFSI was added to the PVdF-HFP acetonitrile solution. The resulting solution was vigorously stirred overnight at room temperature and then cast in a Petri dish by heating at 70 °C and rapidly cooling down to room temperature. The heating-quenching process was repeated until freestanding membranes were obtained; the membranes were finally vacuum dried at 60 °C. All the procedures and material handlings were carried out in an argon-filled dry box. Membranes thickness resulted of around 400 μm, according to the ratio between the amount of starting materials and the capacity of the Petri dish mold. Composition of the membranes here investigated is reported in Table 1. Membranes are named according to the ionic liquid used and the polymer concentration, e.g. P14_20 is based on the PyR14TFSI ionic liquid and 20 wt% polymer.

2.2. Conductivity measurements

The temperature dependence of the ionic conductivity was measured using a Novocontrol broadband dielectric spectrometer in the frequency range 10^{-1}–10^{7} Hz. The liquid samples were placed between stainless steel electrodes with a Teflon spacer (diameter 13.3 mm and thickness 0.97 mm) whereas the membranes were cut into discs (diameter 20 mm and thickness 300–500 μm) and sandwiched between the electrodes. The cell was assembled in argon atmosphere and loaded into a cryo-furnace. Data were collected in the temperature range 110 °C to −55 °C on cooling. A steady flow of nitrogen gas was supplied to the sample holder in order to maintain a dry atmosphere. The DC conductivity was extracted from the low frequency plateau in the frequency dependent conductivity plot.

2.3. Thermal measurements

Differential scanning calorimetry (DSC) experiments were performed using a Q1000 TA instrument. The samples were loaded in hermetic aluminum pans in a glove box. In the experiments the samples were equilibrated at 40 °C, cooled down to −140 °C using a cooling rate of 20 °C min^{-1}, equilibrated at −140 °C, and finally heated from −140 to 120 °C at a rate of 10 °C min^{-1}. The glass transition temperature, T_g, was taken as the midpoint of the heat capacity change from the amorphous glass state to the liquid state, whereas the melting point was taken as the minimum value of the endothermic peak of the melting transition during the heating scans.

2.4. Raman spectroscopy

Raman spectra were recorded on a Bruker IFS66 Fourier Transform spectrometer, equipped with a FRA106 Raman module. The 1064 nm line of a Nd:YAG laser was used as excitation source. The laser power was set to 200 mW, the resolution to 2 cm^{-1}, and the spectra were obtained as the average of over 1000 scans. All Raman spectra were recorded at room temperature.

Table 1
Compositions of the investigated membranes.

Sample	Composition (wt% = weight percentage)
P24_20	20 wt% PVdF-HFP + 80 wt% (0.2 mol kg^{-1} LiTFSI/PyR$_{24}$TFSI)
P24_30	30 wt% PVdF-HFP + 70 wt% (0.2 mol kg^{-1} LiTFSI/PyR$_{24}$TFSI)
P14_20	20 wt% PVdF-HFP + 80 wt% (0.2 mol kg^{-1} LiTFSI/PyR$_{14}$TFSI)
P14_30	30 wt% PVdF-HFP + 70 wt% (0.2 mol kg^{-1} LiTFSI/PyR$_{14}$TFSI)

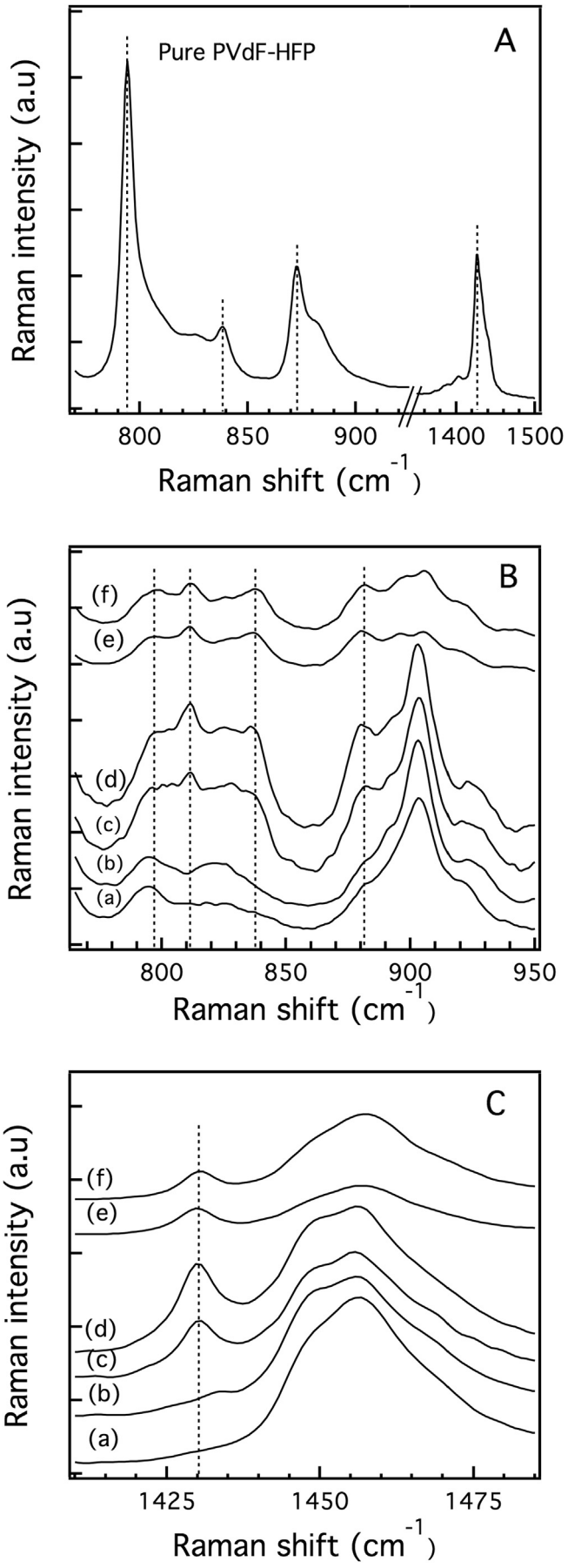

3. Results and discussion

Raman spectra can provide information on both structural changes of the polymer in the membrane and interactions between ionic liquid and the membrane. The original PVdF-HFP powder is semi-crystalline and can be in at least three different crystalline phases according to the polymer chain conformations; Form I, Form II, and Form III [18,19]. The characteristic Raman frequencies for the different phases can be found in literature and involve polymer backbone stretching, skeletal bending, and rocking modes in the frequency range 700–1450 cm^{-1} [19–24]. Fig. 2A shows the characteristic Raman assignments at 795 cm^{-1} (a combination of CH_2 rocking and CF_2 stretching modes), 873 cm^{-1} (a combination of CC symmetric stretching and CCC skeletal bending modes), and 1426 cm^{-1} (a combination of CH_2 scissoring and CH_2 wagging modes) for the crystalline Form II and, at 836 cm^{-1} (CH_2 rocking mode) for the crystalline Form I of pure PVdF-HFP [21,22]. Fig. 2B and C show the changes of these modes in the gel polymer membranes and are discussed further below. Here (only in B and C) Raman spectra of the neat IL/LiTFSI mixtures are also included for better comparison and no interference is found in the region of the characteristic Raman bands for PVdF-HFP.

It is clear from Fig. 2B that the intensity of Raman band at 795 cm^{-1} has decreased in the spectra of the membranes in favor of the band at 836 cm^{-1}. This indicates that the crystalline Form II with a TGTG′ (trans-gauche-trans-minus gauche) conformation, has transformed in to the crystalline Form I with a planar (all trans) conformation [20,24]. Furthermore the strong Raman band for pure PVdF-HFP powder found at 873 cm^{-1}, related to the crystalline Form II [21] has shifted to 880 cm^{-1} for the membranes, a characteristic of the crystalline Form III [25]. In addition, a new band at 810 cm^{-1} can be observed for the membranes also pointing toward the presence of the crystalline Form III [25]. These results, and the absence of other intense Raman bands related to the crystalline Form II (not shown) in the membranes, indicate that crystalline Forms I and III are the dominating phases in our gel polymer electrolytes. However, the band at 1426 cm^{-1} has moved to a slightly higher frequency and is found at 1430 cm^{-1} (Fig. 2C) suggesting the presence of minor amounts of crystalline Form II [22]. A similar behavior was previously found in PVdF/PAN based proton conducting membranes [23] and ionic liquids doped PVdF-HFP proton conducting membranes [20]. In addition, we can observe a weak, but noticeable, influence on the bands belonging to the different crystalline forms by the ionic liquid cation type (see spectra of c, d, e, and f in Fig. 2B). The intensity ratio between the two bands at 810 cm^{-1} and 836 cm^{-1} is significantly lower and the band at 836 cm^{-1} is much broader for the $PyR_{24}TFSI$ based systems compared to systems based on $PyR_{14}TFSI$. These results indicate that the fraction of crystalline Form I is higher compared to Form III in the GPEs based on $PyR_{24}TFSI$ ionic liquid.

Information on the state of the polymer matrix can also be obtained from DSC. Fig. 3 shows the DSC thermograms of the studied membranes, where the DSC thermograms of the neat IL/LiTFSI mixtures are also included for comparison. In the high temperature region of the DSC traces, a broad feature is observed around 100 °C for the GPE membranes that can be attributed to the melting of the semi-crystalline phase of the polymer. The melting temperatures of the GPE membranes are shown in Table 2 and it is clear that the melting temperature decreases significantly compared to the pure

Fig. 2. (A) Raman spectrum of pure PVdF-HFP powder. (B) and (C) Assignments for the Raman active modes of PVdF-HFP in gel polymer electrolytes (vertically dashed lines), (a) $PyR_{14}TFSI$/LiTFSI, (b) $PyR_{24}TFSI$/LiTFSI, (c) P14_30, (d) P14_20, (e) P24_20, and (f) P24_30.

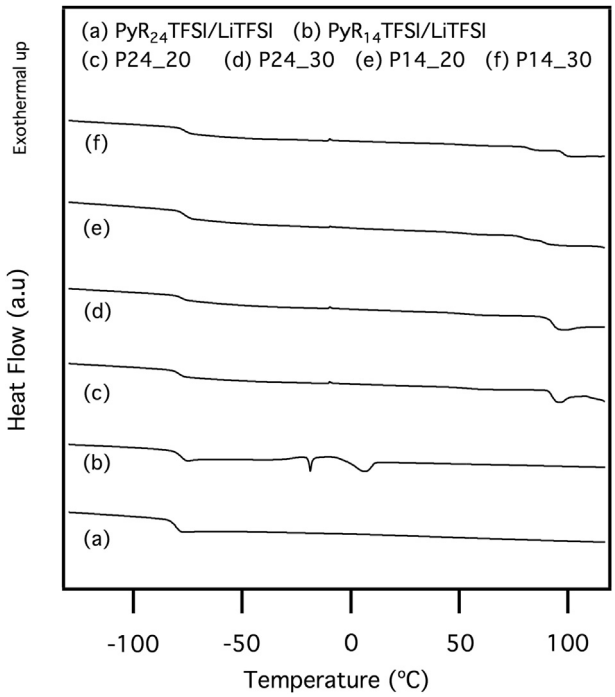

Fig. 3. DSC thermograms of the investigated IL/LiTFSI mixtures, and their gel polymer electrolytes.

PVdF-HFP found around 142 °C (not shown). The broad melting peak and lowering of T_m observed here has previously been found for other ionic liquid/LiTFSI/PVdF-HFP systems [12,13]. The melting transition is further suppressed when the LiTFSI/IL content increases and it has been suggested that this is related to different interactions of Li-salt, IL, and PVdF-HFP [12]. The very weak melting signature around 100 °C, compared to the very pronounced melting peak for the starting PVDF-powder (not shown), also indicates that the degree of crystallinity of the polymer matrix decreases in the membrane configuration.

From the Raman data we can also obtain information on the microscopic state of the ionic liquid in the membrane. In particular the intense Raman band found at 740 cm^{-1}, related to the expansion–contraction mode of the entire TFSI anion, is very sensitive to the ion–ion interactions and conformational changes of the anion [26,27]. Thus this band is a good probe for the influence of confinement or the polymer–ionic liquid interaction. This frequency region is also free from the influence of the IL cation [27] and the PVdF-HFP (see Fig. 4A). The TFSI anion exists in two conformations i.e. the cisoid form (C_1 symmetry) and the transoid form (C_2 symmetry) [26,27]. For the LiTFSI doped ionic liquids, where the anions are fully solvated by the cations and exist as C_1 and C_2 symmetry, the spectral components are found at 738–742 cm^{-1}, whereas for anions interacting with Li-ion (C_{coord}), a spectral component appears in the range 744–748 cm^{-1} [28,29]. Taking this into account we analyze the Raman spectra of the membranes and compare the results to the neat IL/LiTFSI mixtures. The experimental data are fitted using three Voigt components related to C_1, C_2, and C_{coord} component and the results are summarized in Table 3.

Raman spectra in the range 725–760 cm^{-1} are displayed in Fig. 4A for the membranes and IL/LiTFSI mixtures. In the figure raw-data, non-normalized, is shown. Fig. 4B and C show the experimental data (open circles) together with the best fits (solid lines), and the three individual Voigt components C_1, C_2, and C_{coord} (dashed lines) of the $PyR_{24}TFSI$/LiTFSI mixture and the membrane P24_20 respectively. The same analysis is done for the $PyR_{14}TFSI$/LiTFSI mixture and the other membranes. The position of the Raman band of the C_{coord} component is slightly lower in the spectrum from the membranes compared to the position found for the neat IL/LiTFSI mixtures. Also the fraction of Li-ion coordinated anions decreases in the membranes. The decrease in the position of the Raman band and the lower number of anions coordinated to Li-ion points toward a slight decrease in the interaction between Li^+ and $TFSI^-$ in the membranes. The decrease in this Li^+:TFSI interactions can explain the previously found improvement of the Li-ion transport number observed by NMR for a system based on a PVdF-HFP matrix doped with N-ethyl-N-butylpiperidinium bis(-trifluoromethanesulfonyl)imide (PP24TFSI) ionic liquid and the LiTFSI salt [12].

In addition to Li-ion coordinated anions, the behavior of the weakly coordinated, or free, anions also change in the membranes, compare C_1 and C_2 components of Fig. 4B and C and Table 3. In the neat IL/LiTFSI mixtures the difference between the C_1 and C_2 components are higher than in the membranes. This change in the conformation can be a result of ionic liquid polymer interactions. The influence on the IL/LiTFSI mixture by the confinement in the membrane is also observed in the DSC data. In the DSC trace of $PyR_{14}TFSI$/LiTFSI shows an endothermic feature around −20 °C in addition to the melting peak related to a solid–solid phase transition is found [30]. In Fig. 2 we can see that the tendency for crystallization of $PyR_{14}TFSI$/LiTFSI mixture is suppressed by the incorporation into the membrane. A clear signature of a glass transition in the low temperature region is found in the DSC traces for all membranes. However, no melting transitions are observed for the IL/LiTFSI mixtures in the membranes. The observed glass transition temperatures (T_g) in the membranes are slightly higher than the T_g values found for the neat IL/LiTFSI mixtures (Table 2). These results indicate that there is a small but clear influence on the physical properties of the ionic liquid by the confinement in the membrane, in agreement with the Raman results. The polymer concentration in the membrane is here too low to result in a large change in T_g in agreement with previously reported results for ionic liquids swollen PVdF-HFP systems [20,31].

The temperature dependence of the ionic conductivity of the ionic liquid based gel polymer electrolytes is shown in Fig. 5. The ionic conductivity of the IL/0.2 mol kg^{-1} LiTFSI mixtures are included for comparison. The room temperature ionic conductivity values for the IL/LiTFSI mixtures are in excellent agreement with the values reported in the literature [17,30]. For the $PyR_{14}TFSI$/LiTFSI mixture, the ionic conductivity can only be measured down to −33 °C since the sample crystallizes and a constant plateau for the DC conductivity cannot be observed in the investigated frequency range. However, the tendency of crystallization of the $PyR_{14}TFSI$/LiTFSI ionic liquid electrolyte is suppressed in the membranes in agreement with the DSC results. The ionic conductivity here follows the typical non-Arrhenius behavior of liquid electrolytes and can be well described by a VTF (Vogel–Tammann–Fulcher) function

Table 2
Glass transition temperature (T_g), ideal glass transition temperature (T_0), fragility parameter (D), melting temperature (T_m), and ionic conductivity at 27 °C for the investigated IL/LiTFSI mixtures and membranes.

Sample	T_g (°C)	T_0 (°C)	D	T_m (°C)	$\sigma_{27°C}$ (mS cm^{-1})
$PyR_{24}TFSI$/LiTFSI	−81	−107	4.5	–	1.6
P24_20	−79	−111	6.6	96	0.5
P24_30	−78	−112	6.7	97	0.5
$PyR_{14}TFSI$/LiTFSI	−79	−109	5.2	5	1.6
P14_20	−76	−115	6.2	97	0.8
P14_30	−76	−115	6.5	99	0.6

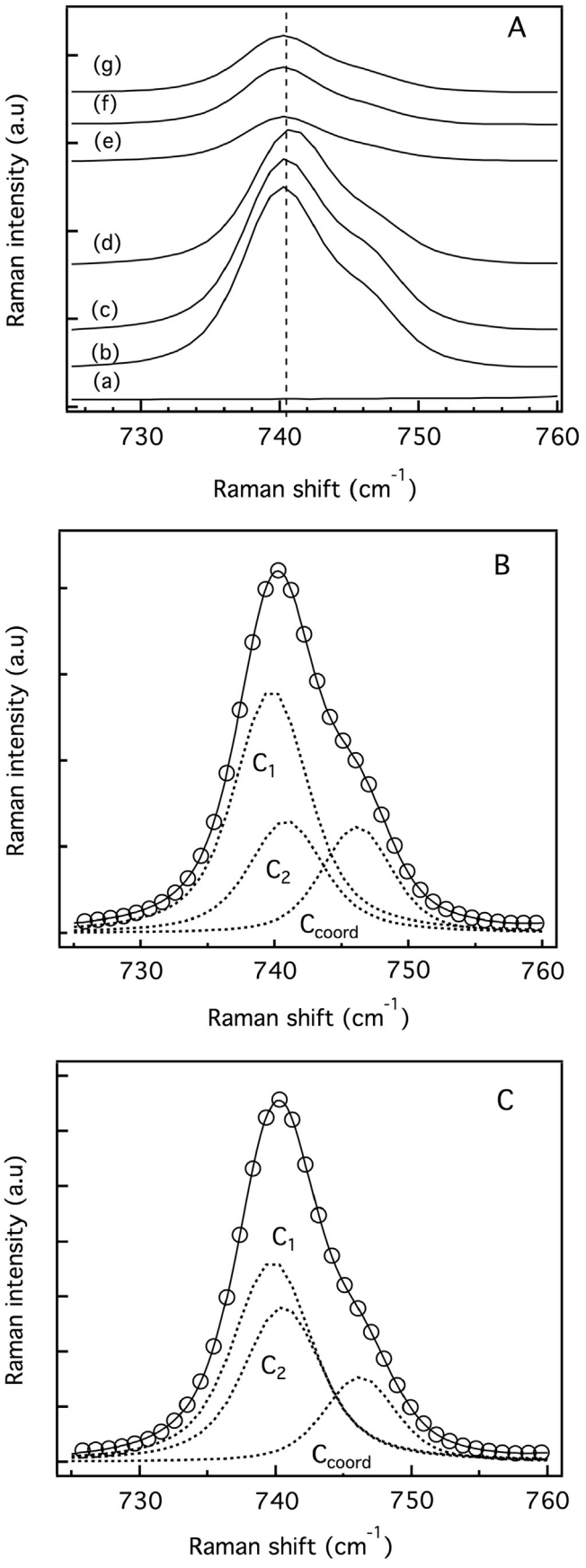

Fig. 4. (A) Raman spectra, non-normalized, of the studied samples: (a) pure PVdF-HFP, (b) $PyR_{24}TFSI/LiTFSI$, (c) $PyR_{14}TFSI/LiTFSI$, (d) P14_30, (e) P14_20, (f) P24_20 and (g) P24_30. Fitting results: (B) $PyR_{24}TFSI/LiTFSI$ and (C) P24_20. The experimental spectra (open circles) are shown together with the best fits (solid lines) and the individual Voigt components for C_1, C_2 and C_{coord} (dashed lines).

Table 3
Position of the Raman shift (ν) and the percentage of the relative integrated areas (A) of the three components (C_1, C_2, and C_{coord}).

Sample	ν-C_1	A-C_1	ν-C_2	A-C_2	ν-C_{coord}	A-C_{coord}
$PyR_{24}TFSI/LiTFSI$	739.8	54	741.7	25	746.4	21
P24_20	739.8	47	740.6	36	746.1	17
P24_30	739.8	49	740.7	35	746.1	16
$PyR_{14}TFSI/LiTFSI$	739.9	55	742	24	746.3	21
P14_20	740	48	740.5	36	746.1	16
P14_30	740	49	740.5	35	746	16

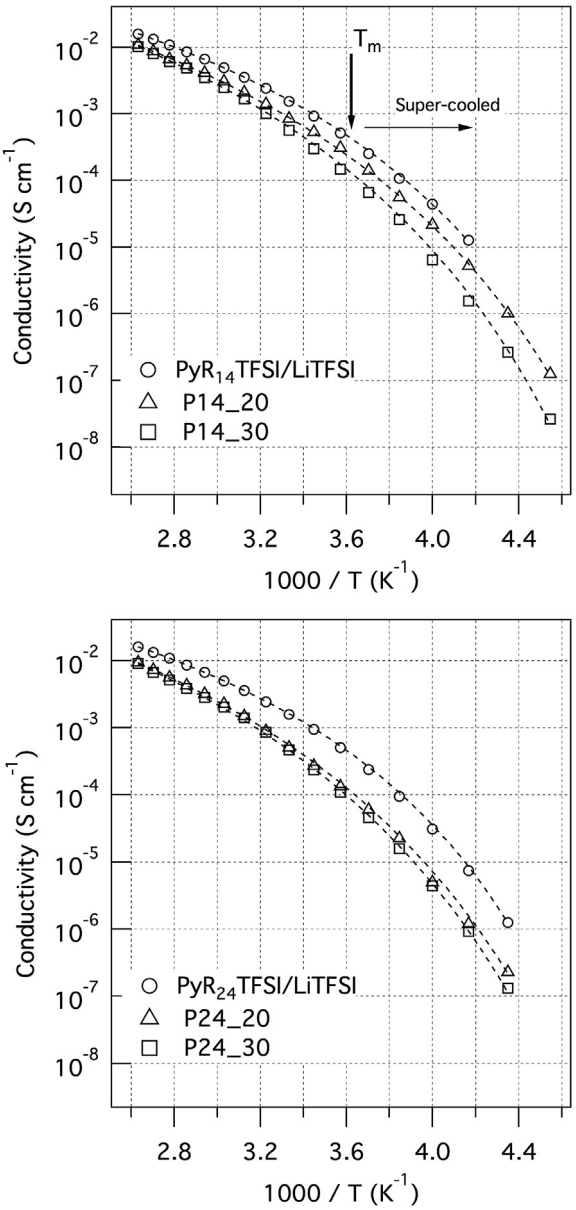

Fig. 5. Temperature dependence of the ionic conductivity of the neat IL/LiTFSI mixtures and the gel polymer electrolyte membranes. Dotted lines are fits to the VTF equation, eq. (1). For the PyR14TFSI/LiTFSI mixture the melting point, defining the onset of the super-cooled liquid state, is indicated in the figure.

$$\sigma = \sigma_0 exp - \left(\frac{DT_0}{T - T_0}\right) \quad (1)$$

where σ_0 is the conductivity at infinite temperature, D is a constant and inversely proportional to the fragility of the liquid, and T_0 is related to an ideal glass transition temperature [32]. The fragility defines the temperature dependence of transport properties, such as conductivity and viscosity, near to the glass transition temperature and is dependent on the interactions of the system [31,32]. Table 2 summarizes the D and T_0 values obtained from the ionic conductivity fits to the VTF equation, eq. (1). The VTF behavior indicates that the ion transport is controlled by the viscous properties of the liquid.

From Fig. 5, it is clear that the ionic conductivity of IL/LiTFSI mixtures is higher than that of the corresponding GPE membranes for both investigated systems. This decrease in conductivity can be due to both lower fraction of the conducting component i.e. the IL/LiTFSI mixture present in the membrane and/or interactions between the IL/LiTFSI mixture and the polymer matrix. To get a further insight on this issue, we can look at the D parameters obtained from VTF fitting. It is clear from the values shown in Table 2 that the D value increases when the liquid electrolytes are incorporated into the membranes in both systems, with a slightly larger increase for the $PyR_{24}TFSI$/LiTFSI mixture. The increase in the D parameter indicates an increase in the interaction in the liquid phase. Thus, it is evident that the confinement in the matrix has affected the basic physical properties of IL/LiTFSI mixture following the T_g increment discussed above.

4. Conclusions

In this work, we investigated transport properties, thermal properties, structure, and interactions of Li-ion conducting gel polymer electrolytes based on PVdF-HFP copolymer. The Li-ion conduction was obtained by incorporating IL/LiTFSI solutions, based on pyrrolidinium cation family and the TFSI anion, in to the matrix. We observed that the physical properties of IL/LiTFSI mixtures are clearly influenced by the confinement matrix with an increase in the glass transition temperature, change in the coordination and conformation in the IL/LiTFSI mixtures and a change of the fragility parameter. We see that the degree of crystallinity of pure PVdF-HFP decreases with the doping of IL/Li–salt mixtures and that the PVdF-HFP polymer matrix preferentially adopts the crystalline Form I and III.

Acknowledgment

We kindly acknowledge the financial support from the Swedish Research Council and the National Graduate School for Materials Science. The results of this work have been obtained by the financial support of the European Community within the Seventh Framework Programme APPLES (Advanced, High Performance, Polymer Lithium Batteries for Electrochemical Storage) Project (contract number 265644).

References

[1] E. Quartarone, P. Mustarelli, Chem. Soc. Rev. 40 (2011) 2525–2540.
[2] J.Y. Song, Y.Y. Wang, C.C. Wan, J. Power Sources 77 (1999) 183–197.
[3] G. Li, Z. Li, P. Zhang, H. Zhang, Y. Wu, Pure Appl. Chem. 80 (11) (2008) 2553–2563.
[4] A.M. Stephan, Eur. Polym. J. 42 (2006) 21–42.
[5] S.S. Sekhon, B.S. Laila, J.-S. Park, C.-S. Kim, K. Yamada, J. Mater. Chem. 16 (2006) 2256–2265.
[6] M.A.K.L. Dissanayake, L.R.A.K. Bandara, R.S.P. Bokalawala, P.A.R.D. Jayathilaka, O.A. Ileperuma, S. Somasundaram, Mater. Res. Bull. 37 (2002) 867–874.
[7] Y. Wang, Solar Energy Mater. Solar Cells 93 (2009) 1167–1175.
[8] L.N. Sim, S.R. Majid, A.K. Arof, Solid State Ionics 209-210 (2012) 15–23.
[9] J.M. Tarascon, A.S. Gozdz, C. Schmutz, F. Shokoohi, P.C. Warren, Solid State Ionics 49 (1996) 86–88.
[10] M. Armand, F. Enders, D.R. McFarlane, H. Ohno, B. Scrosati, Nat. Mater. 8 (2009) 621.
[11] H. Ye, J. Huang, J.J. Xu, A. Khalfan, S.G. Greenbaum, J. Electrochem. Soc. 154 (11) (2007) A1048–A1057.
[12] A. Fernicola, F.C. Weise, S.G. Greenbaum, J. Kagimoto, B. Scrosati, A. Soleto, J. Electrochem. Soc. 156 (7) (2009) A514–A520.
[13] C. Sirisopanaporn, A. Fernicola, B. Scrosati, J. Power Sources 186 (2009) 490–495.
[14] J.-K. Kim, A. Matic, J.-H. Ahn, P. Jacobsson, J. Power Sources 195 (2010) 7639.
[15] S. Ferrari, E. Quartarone, P. Mustarelli, A. Magistris, M. Fagnoni, S. Protti, C. Gerbaldi, A. Spinella, J. Power Sources 195 (2010) 559–566.
[16] M.A. Navarra, J. Manzi, L. Lombardo, S. Panero, B. Scrosati, ChemSusChem 4 (2011) 125–130.
[17] A. Fernicola, F. Croce, B. Scrosati, T. Watanabe, H. Ohno, J. Power Sources 174 (2007) 342–348.
[18] Y. Yang, S. Ramalingam, G. Wu, S.L. Hsu, L.W. Kleiner, F.-W. Tang, N. Ding, S. Hossainy, Polymer 49 (2008) 1926–1933.
[19] M. Kobayashi, K. Tashiro, H. Tadokoro, Macromolecules 8 (2) (1975) 158–171.
[20] A. Martinelli, A. Matic, P. Jacobsson, L. Börjesson, M.A. Navarra, S. Panero, B. Scrosati, J. Electrochem. Soc. 154 (8) (2007) G183–G187.
[21] R.D. Simoes, A.E. job, D.L. Chinaglia, V. Zucolotto, J.C. Camargo-Filho, N. Alves, J.A. Giacometti, O.N. Oliveira Jr., C.J.L. Constantino, J. Raman Spectrosc. 36 (2005) 1118–1124.
[22] M.A. Bachmann, J.L. Koenig, J. Chem. Phys. 74 (10) (1981) 5896–5910.
[23] A. Martinelli, M.A. Navarra, A. Matic, S. Panero, P. Jacobsson, L. Börjesson, B. Scrosati, Electrochim. Acta 50 (2005) 3992–3997.
[24] T. Boccaccio, A. Bottino, G. Capannelli, P. Piaggio, J. Membr. Sci. 210 (2002) 315–329.
[25] K. Tashiro, M. Kobayashi, H. Tadokoro, Macromolecules 14 (6) (1981) 1757–1764.
[26] M. Herstedt, M. Smirnov, P. Johansson, M. Chami, J. Grondin, L. Servant, J.C. Lassegues, J. Raman Spectrosc. 36 (2005) 762.
[27] A. Martinelli, A. Matic, P. Johansson, P. Jacobsson, L. Börjesson, A. Fernicola, S. Panero, B. Scrosati, H. Ohno, J. Raman Spectrosc. 42 (2011) 522–528.
[28] J.C. Lassègues, J. Grondin, C. Aupetit, P. Johansson, J. Phys. Chem. A 113 (2009) 305.
[29] J. Pitawala, J.-K. Kim, P. Jacobsson, V. Koch, F. Croce, A. Matic, Faraday Discuss 154 (2012) 71.
[30] A. Martinelli, A. Matic, P. Jacobsson, L. Börjesson, A. Fernicoal, B. Scrosati, J. Phys. Chem. B 113 (2009) 11247.
[31] A. Martinelli, A. Matic, P. Jacobsson, L. Börjesson, A. Fernicola, S. Panero, B. Scrosati, H. Ohno, J. Phys. Chem. B 111 (2007) 12462–12467.
[32] J. Leys, M. Wübbenhorst, C.P. Menon, R. Rajesh, J. Thoen, C. Glorieux, P. Nockemann, B. Thijs, K. Binnemans, S. Longuemart, J. Chem. Phys. 128 (2008) 064509.